ACS Photonics

Article

pubs.acs.org/journal/apchd5

Plasmonically Enhanced Chiral Optical Fields and Forces in Achiral Split Ring Resonators

M. H. Alizadeh*,[†,‡] and Björn M. Reinhard*,[‡,§]

[†]Department of Physics, [§]Department of Chemistry, and [‡]The Photonics Center, Boston University, Boston, Massachusetts 02215, United States

ABSTRACT: The two enantiomers (mirror images) of a biomolecule can show drastically different behaviors, requiring the development of sensitive approaches for their identification and separation. Plasmonic nanostructures have shown promise for enhancing the sensitivities of chiral spectroscopies, but the generation of chiral near fields with a specific handedness in the spatial domain surrounding the plasmonic structures remains a challenge. Here we demonstrate that achiral bianisotropic structures, which couple the electric and magnetic fields, can achieve high enhancements of optical chirality in an extended spatial region. Magneto-electric coupling in such structures facilitates electrically excited magnetic resonances in the near IR and optical regimes, which in turn can result in highly enhanced optical chirality in an extended region of space. We apply this concept to achiral double split ring resonators (DSRRs) and demonstrate their potential in generating enhanced chiral fields and forces. Also, the behavior of optical chirality density gradient and chirality flux in such structures is examined, and it is shown that plasmonically generated chiral forces may pave the way to a new class of chiral biosensors.

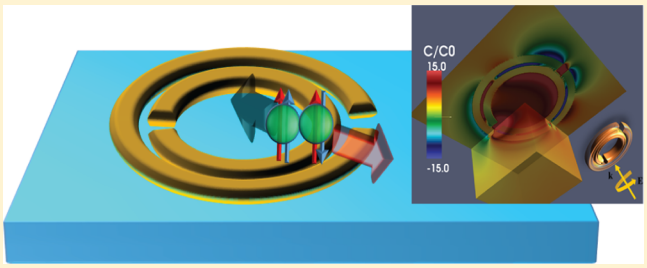

KEYWORDS: *optical chirality, bianisotropy, circular dichroism, chiral forces, metamaterials*

An object is chiral if it cannot be mapped to its mirror image by rotations and translations alone. Chiral molecules can exist a priori in two nonsuperimposable mirror images, that is, enantiomeric forms. Enantiomers can differ in their chemical behavior and reactivity, which can have drastic consequences. In drugs, for instance, one enantiomer may have a desired physiologic effect, while the other enantiomer can be inactive or even harmful. The most infamous example is thalidomide ("contergan"), for which one enantiomer is an effective sedative, whereas the other is teratogen. Administration of the racemic mix to pregnant women led to the birth of thousands of children with malformed limbs.[1] This example illustrates the need for highly sensitive detection of chiral biomolecules in research and drug development. Chemical enantiomers have long been distinguished through their optical activity.[2] The interaction between a molecule with a given chirality and electromagnetic (EM) fields depends strongly on the degree of chirality of the EM field, a measure for which was introduced by Lipkin.[3] Such interactions are utilized in circular dichroism (CD) spectroscopy, which is the dominant tool to detect and characterize chiral biomolecules.[4] In this technique the difference in optical excitation of a chiral molecule by left and right circularly polarized light (CPL) is recorded. It is now understood that the field enhancement provided by plasmonic nanostructures can facilitate the generation of local optical chirality densities larger than the local optical chirality of CPL. Tang and Cohen introduced the concept of optical chirality as a measure of the local chiral density of the electromagnetic field and demonstrated the possibility of generating light with enhanced enantioselectivity which they dubbed "super-chiral" light.[5,6] The definition of optical chirality density of the electromagnetic field at a frequency ω, $K = -(\varepsilon_0\omega/2)\mathrm{Im}(\boldsymbol{E}^*\cdot\boldsymbol{B})$, where $\boldsymbol{E}$ and $\boldsymbol{B}$ are the complex electric and magnetic fields, respectively, implies that K can be enhanced through correct alignment of the strong evanescent $\boldsymbol{E}$- and $\boldsymbol{H}$-fields around plasmonic structures.[7−10] If we assume that the optical response of the plasmonic structure is not appreciably altered in the presence of a chiral molecule it can be shown that CD $\propto -4/\varepsilon_0\mathrm{Im}(\chi)$, where χ is the electric-magnetic dipole polarizability of the chiral molecule.[5,6,11] So it is readily concluded that by enhancing optical chirality density one can achieve an enhanced CD signal. However, there are two major obstacles in such enhancement schemes. First, it has proven challenging to generate evanescent enhanced chiral fields with uniform sign of optical chirality over large areas in the vicinity of metal nanostructures.[11−15] This problem is a consequence of the dominant electric dipole character of optically active modes in conventional plasmonic structures. Second, most of the focus in the literature has been on utilizing chiral structures to generate chiral near-fields. While this approach is, in principle, feasible[7] in applications that seek to achieve enhanced chiral molecular signals, the need for separating the optical activity stemming from molecules from that of a chiral structure introduces additional experimental complexity. Usually one will have to subtract a molecular CD signal from that of a chiral metal structure background. A series of geometries have been devised

Received: October 27, 2014
Published: February 23, 2015

DOI: 10.1021/ph500399k
ACS Photonics 2015, 2, 361−368

to alleviate the first problem, including three-dimensional (3D) helical metal structures[16] and negative refractive index fish-net structures.[17] Such structures can provide relatively large regions of uniform-sign chiral near-field. However, due to their three-dimensional nature their fabrication, especially for the operation in the visible range of the electromagnetic spectrum, is involved. In addition, the degree of enhancements reported for these structures is quite low. Garcia-Etxarri and Dionne demonstrated that isotropic nanostructures sustaining optical-frequency magnetic and electric resonances can yield a globally enhanced optical chirality.[11] The proposed materials utilized, however, Mie resonances of a high-refractive index spherical particle, which generate only modest electromagnetic field enhancements. Consequently, the obtained degree of local chirality enhancement and its spatial extension were intrinsically limited. Here we show that achiral bianisotropic plasmonic structures, which couple the electric and magnetic fields, achieve high enhancements of optical chirality in an extended spatial region. We demonstrate that the magneto-electric coupling in such structures facilitates electrically excited magnetic resonances in near IR and optical regimes, which in turn can result in highly enhanced optical chirality in an extended region of space. We apply this concept to achiral split ring resonators (SRRs) and demonstrate their potential for generating enhanced chiral fields and forces.

RESULTS AND DISCUSSION

Double split ring resonators (DSRRs) are best known in the context of metamaterials as the benchmark for negative refractive index and left-handed materials.[18] The DSRR, Figure 1, is composed of two conducting rings of metal with gaps on opposite sides. The rings possess self-inductance, L, and the gap in the rings creates a capacitance, C. Thus, the DSRR forms an RLC resonator, with resonance frequency at $\omega_0 = (1/(LC)^{1/2})$.[19,20] Despite the seemingly straightforward physics of DSRRs, subtle effects can be generated depending on the angle of the incident wave and its polarization. It is well-understood that DSSRs are bianisotropic structures, with magneto-electric coupling through cross-polarization terms.[21−23] Simultaneous electric and magnetic resonances of the structure, due to its bianisotropy, can be a basis for new optical chirality enhancement schemes. To account for the magneto-electric coupling, one can use the general constitutive relations:[23] $\boldsymbol{D} = \varepsilon\varepsilon_0\boldsymbol{E} - i(\varepsilon_0\mu_0)^{1/2}\gamma\boldsymbol{H}$ and $\boldsymbol{B} = \mu\mu_0\boldsymbol{H} + i(\varepsilon_0\mu_0)^{1/2}\gamma^T\boldsymbol{E}$, where γ is the magneto-electric coupling tensor. Traditionally, DSRRs have mostly been investigated in the GHz and THz regimes. Extending this concept to the IR and optical regimes poses several difficulties.[24−29] In the IR and especially in the visible spectral range metals are no longer ideal conductors. The frequency of the EM wave is close to the plasma frequency of the metal and the role of the imaginary part of the complex permittivity is more pronounced. In addition, in the GHz and THz regimes magnetic resonances of the DSRR arising from nonzero normal component of the incident $\boldsymbol{H}$-field are much stronger than those stemming from modes excited through the $\boldsymbol{E}$-field component.[30] Such magnetic resonances are the cornerstone for negative permeability. This is not a priori the case in the optical regime where strong plasmonic resonances can be generated and one should incorporate the nontrivial kinetic inductance into L and additional surface contributions into the capacitance C.[24−27] Furthermore, in the IR and visible regimes even normal incident EM fields with no magnetic flux through the DSRR can excite magnetic resonances.[24] In ref 27, it is demonstrated that in U-shaped SRRs illuminated by normally incident, linearly polarized light, magnetic modes contain an odd number of half-wavelengths of the current density within the ring, whereas electric resonances correspond to integer numbers of the full wavelength.[27] The focus in these studies have, however, been on U-shaped SRRs, which are composed of three legs. Each of these legs is considered a single resonator that can sustain independent modes. However, the DSRR considered here comprises two monolithic rings, each of which is a single resonator. In addition, due to close proximity of the double rings in the DSRR, mode hybridization and also stronger resonances are expected. To gain insight into the nature of the resonances in this design we performed a series of full wave, finite-difference time-domain simulations for different polarization conditions. The structure is embedded in vacuum and periodic boundary conditions are applied. The inner ring of the investigated DSRR has an inner radius of 130 nm and an outer radius of 160 nm with a gap size of ten degrees and a thickness of 30 nm. The outer ring has an inner radius of 170 nm and an outer radius of 200 nm. The gap opening is the same as that of the inner radius. Gold was chosen as the material and the optical constants were extracted from Johnson and Christy.[31] $\boldsymbol{E}$- and $\boldsymbol{H}$-field distributions for the SRR at λ = 1258 nm are illustrated in Figure 1. This wavelength was chosen because it is close to the magnetic quadruple mode. Also, at this wavelength an extended, uniform-sign chiral near field is generated around the DSRR. To keep our analysis intuitive, we first treat the resonators separately and focus on the outer ring (OR) assuming an incident $\boldsymbol{E}$-field polarization perpendicular to the SRR gap. This is demonstrated in Figure 2a, where transmissions for two different incident $\boldsymbol{k}$-vector orientations are shown. In the first case, the incident $\boldsymbol{k}$-vector is normal to the SRR plane and there is no incident magnetic flux through the ring. As the incident light preserves the symmetry of the SRR, it does not couple to the capacitive mode of the gap and consequently will not excite the fundamental magnetic mode.[24] However, with the same polarization but with the $\boldsymbol{k}$-vector parallel to the SRR plane, the normal $\boldsymbol{H}$-vector penetrates the ring and extra modes are excited which are magnetic in nature. We confirmed this by finding the distribution of the current density ($\boldsymbol{J}$) in the ring. As it is seen in Figure 2a, the only

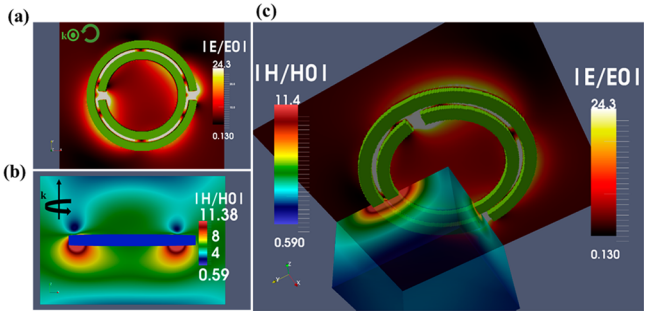

Figure 1. (a) Map of the simulated electric field enhancement ($|\boldsymbol{E}/\boldsymbol{E}_0|$) for the investigated DSRR (see text) at λ = 1258 nm. The highest $\boldsymbol{E}$-field is observed in the gap between the rings as well as the capacitive gaps. (b) Map of the simulated magnetic field enhancement ($|\boldsymbol{H}/\boldsymbol{H}_0|$) for the DSRR at λ = 1258 nm. The largest enhancement occurs inside the DSRR close to the inner ring and spreads inside the enclosed area. (c) Bird's-eye view of $|\boldsymbol{E}/\boldsymbol{E}_0|$ and $|\boldsymbol{H}/\boldsymbol{H}_0|$ distributions. The polarization of the incident wave is as (a).

DOI: 10.1021/ph500399k
ACS Photonics 2015, 2, 361−368

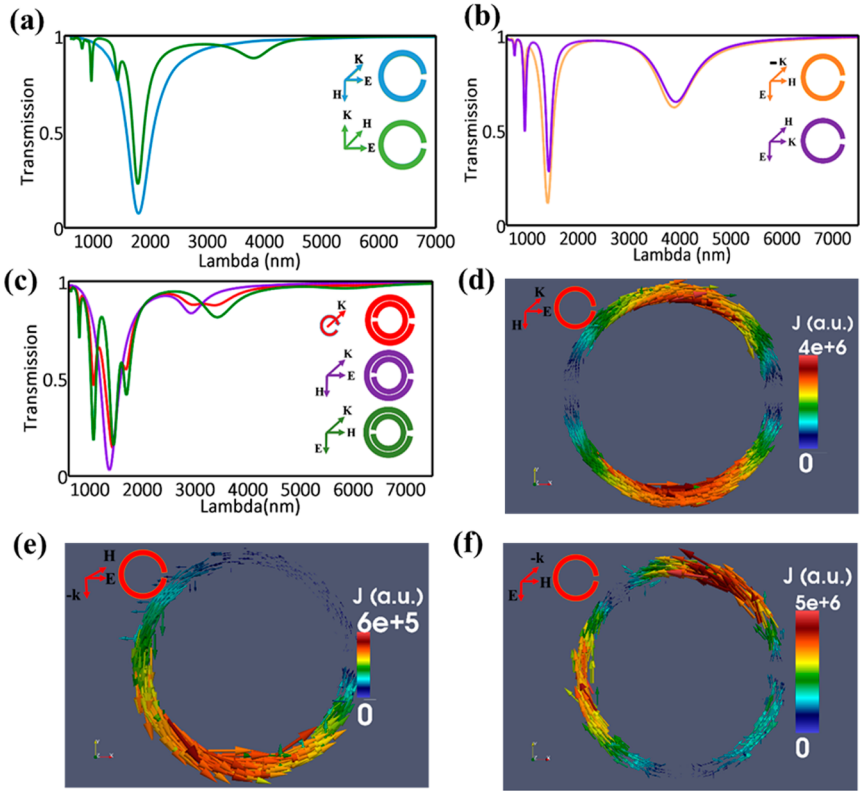

Figure 2. (a) Transmission spectra for the investigated SRR (see text) for two different incident ***k***-vectors (see insets). In both cases the incident light is polarized along the *x*-axis perpendicular to the gap. (b) In the case of zero magnetic flux, *y*-polarized incident light couples to the magnetic modes as is evident from the degeneracy of the modes excited by two polarizations of incident light (see insets). (c) Transmission spectra of the SRR for normal incident light with circular polarization (red) and with two orthogonal linear polarizations (purple and green). (d–f) Current density (***J***) distributions for different resonances. The current density map is plotted for the electric resonance at λ = 1782 nm in (d) and for the magnetic resonances at λ = 3805 and 1010 nm, in (e) and (f), respectively. ***J*** spans a full wavelength around the ring in (d), half wavelength in (e), and three half wavelengths in (f).

excited mode in the case of zero magnetic flux (blue line) is at 1782 nm when ***J*** (Figure 2d) spans a full wavelength around the ring. This is physically intuitive, as in such a case the maximum net dipole moment of the ring is produced and couples efficiently to the external field. The net current flowing in the ring, however, is virtually zero, hindering any magnetic resonances. In the second scenario (green line in Figure 2a), with a nonzero magnetic flux through the ring, additional modes besides the fundamental electric mode are excited. In this case, the first mode at 3805 nm is the fundamental magnetic mode for which ***J*** forms a half wavelength standing wave in the resonator (Figure 2e). This corresponds to an asymmetric charge distribution across the gap. In this situation a net current is induced in the ring and the two sides of the gap are capacitively coupled. The next higher mode at 1782 nm lies at the same wavelength of the electric dipole mode and shows the same ***J*** distribution obtained without net magnetic flux through the ring. It is concluded that for the incident EM wave with an ***E***-component perpendicular to the SRR gap, magnetic resonances are observed only if an ***H***-field component through the ring is present. The situation is starkly different, however, in the case of an incident ***E***-field aligned parallel to the gap. Transmission spectra for two scenarios with orthogonal ***H***-field orientations are shown in Figure 2b. It is evident that the excited modes are degenerate, with only slight differences in their strength. This stems from the ability of the incident ***E***-field to excite the modes with asymmetrical charge distributions across the gap. In the circuit model terminology the asymmetrical charge distribution induced by the incident ***E***-field renders a nonzero capacitance across the gap, which can couple to the inductive modes of the ring resonator. The ***J*** distribution of the mode at λ = 1070 nm (Figure 2f) for such a polarization contains three half wavelengths, consistent with the current density distribution for the quadruple magnetic resonance.

If one adds the inner ring and introduces CPL for excitation, mode hybridization between inner and outer rings of the DSRR as well as the superposition of modes excited by *x*- and *y*-polarized waves result in additional features and spectral shifts. This is demonstrated in Figure 2c, where the transmission spectra for the DSRR under different polarizations are plotted. We ensure that electrically excited magnetic modes are present in the DSRRs throughout the remaining part of our manuscript by using CPL under normal incidence. This is especially significant as the excited modes give rise to strong magnetic responses, which in turn will result in chiral enhancement even at frequencies that do not fall near any electric dipolar resonances. This is a departure from conventional schemes of enhancement, which mainly rely on modes which are electric in nature.

Comparison between the CD Signals from Gammadion and DSRR. Despite having anisotropic and bianisotropic properties,[21,23] the DSRR is not geometrically chiral. Consequently, we expect that the DSRR, despite generating enhanced chiral near fields, will not contribute to the total detected CD signal. To test this, the absorptions under normal

DOI: 10.1021/ph500399k
ACS Photonics 2015, 2, 361–368

incident right circularly polarized light (RCPL) and left circularly polarized light (LCPL) were calculated, and the CD spectrum was determined as the difference between the two absorption spectra. We performed this analysis for the DSRR as well as for a chiral reference structure. For the latter, we chose a Gammadion, Figure 3a, which is an intensely studied chiral

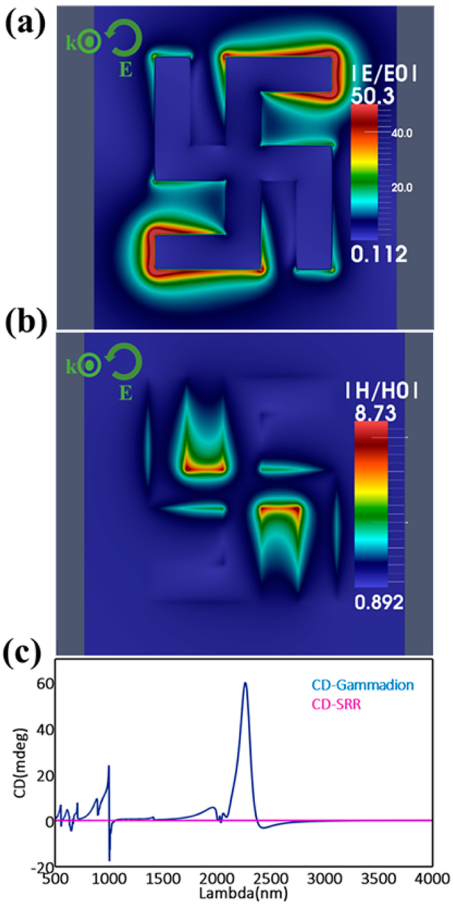

Figure 3. (a) Map of the simulated electric ($|\boldsymbol{E}/\boldsymbol{E}_0|$) and (b) magnetic ($|\boldsymbol{H}/\boldsymbol{H}_0|$) field enhancement for the Gammadion as described in the text at λ = 2120 nm. While the $\boldsymbol{E}$-field is most strongly localized at the tip of the metal bars, the $\boldsymbol{H}$-field is strongest in the central part of the structure. (c) CD plot of the Gammadion (navy) compared to that of the DSRR (purple).

structure in the literature.[7,15] The width and length of the gammadion, which is made of gold, are 400 nm each with a thickness of 20 nm. The size of the gap between adjacent arms is 80 nm. In Figure 3c, the CD spectra of both DSRR and gammadion are plotted. It is evident that the CD signal from the Gammadion, which has spatial dimensions comparable to those of the DSRR and its plasmonic resonances spectrally overlap with those of the DSRR, is significant while we obtain virtually zero CD signal from the DSRR.

Same-Sign Chiral near Fields Surrounding DSRR. One of the obstacles in using plasmonic structures, such as the Gammadion, as substrates for surface enhanced chiral spectroscopy is the alternating sign of optical chirality, K, around them, which suppresses a net chiral enhancement, unless molecules can be selectively located at specific spots. To overcome this problem, alternative design approaches, including nanobars arranged in a 3D configuration,[14] 3D helices,[16] and high refractive index materials,[11] have been proposed. Each of these proposed designs offers, however, unique challenges for fabrication and practical implementation. For instance, the generation of 3D arranged nanobars requires intricate 3D nanofabrication with precise alignment. For the helices, the incoming wave should be incident at grazing angle and, furthermore, the fabrication of morphologically well-defined 3D helices remains cumbersome. Moreover, the resonance frequencies of such structures normally lie far from the visible and near-infrared regimes, which are desirable spectral ranges for chiral biosensing. Simultaneous electric and magnetic resonances associated with high-refractive index materials offer interesting design options for chiral sensing, but realistic estimates of the achievable enhancements are low due to the lack of strong plasmonic resonances.[11] Achiral DSRRs, which are 2D structures and easy to fabricate in the near-IR and optical regime,[32] are prominent candidates for enhancing chirality as they are bianisotropic structures, which can sustain magneto-electric coupling, hence, strong magnetic responses. The spatial distribution of the electric and magnetic fields of the loop design in DSRR guarantees nonperpendicular components of these fields and together with the intrinsic $\pi/2$ phase difference between the electric and magnetic component in the near field region can result in an extended enhanced optical chirality, K. We emphasize that such alignment is missing in a linear electric dipole, where $\boldsymbol{E}$- and $\boldsymbol{H}$-fields have their local maxima at perpendicular angles (see Figure 3a,b). To validate this intuitive picture of chiral near-field generation in DSRRs, we performed full-wave EM simulations. In the first step, the generation of uniform-sign chiral fields in the vicinity of the DSRR was tested. Before visualizing the optical chirality it was normalized to that of CPL. In Figure 4a, the resulting optical chirality of the DSRR in the xy-plane is shown at λ = 1258 nm. Signs were chosen such that LCPL has positive chirality. The plot confirms the formation of a highly enhanced chiral field of uniform sign inside of the DSRR. In stark contrast to most of the chiral structures studied previously,[7,12−15] the DSRR does not show strong fluctuations in the sign of the optical chirality as a function of spatial angle inside the space enclosed by the DSRR where the optimum alignment of the $\boldsymbol{E}$- and $\boldsymbol{H}$-field is obtained. The distribution of the optical chirality in the xz- and yz-planes are shown in Figure 4b. A bird's eye view of the chirality enhancement is shown in Figure 4c. The relative orientation of the $\boldsymbol{E}$- and $\boldsymbol{H}$-field in these planes facilitates a preservation of chiral field over large regions in space. In order to gain insight into the spectral behavior of chiral enhancement in the DSRR we calculated the chiral enhancement peaks and chiral enhancement at two different points inside the DSRR vs excitation wavelength (Figure 4d,e). The peak chiral enhancement can reach values as high as 45 (Figure 4d). Such highly enhanced chiral fields, however, are largely confined to small areas such as the narrow gaps between the rings and the end-capacitive gaps and are due to the very large field enhancements in such spots. Although the trend of the peaks follows the resonances of the structure (see Figure 2c), they occur slightly off these resonances. For instance, the highest enhancement appears at around λ = 1580 nm instead of at λ = 1420 nm, which is the electric dipole resonance of the DSRR. When the structure is on electric (magnetic) resonance, it acquires additional $\pi/2$ phase delay (advance) with respect to the magnetic (electric) near-field, which destroys the required phase condition and minimizes the chiral enhancement. But when the resonance is passed, the π-phase acquisition of the resonator revives the required phase condition with an opposite

DOI: 10.1021/ph500399k
ACS Photonics 2015, 2, 361−368

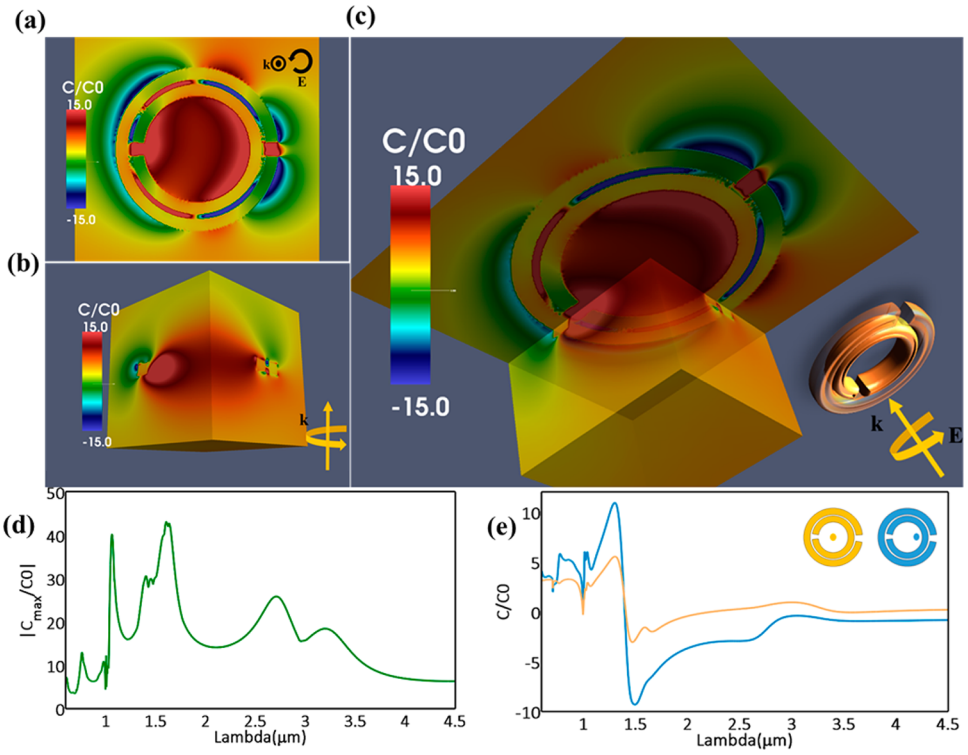

Figure 4. (a) Optical chirality in *xy*-plane at λ = 1250 nm. Inside the DSRR inner ring a uniform-sign enhanced chiral field is generated. (b) Distribution of such field in the *xz*- and *yz*-planes. The enhanced chiral field preserves its sign in a large central volume (c) Bird's-eye view of optical chirality density in the volume surrounding the DSRR. (d) Spectrum of absolute value of peak chiral enhancement vs excitation wavelength. (e) Spectrum of chiral enhancement for two different spots inside the DSRR.

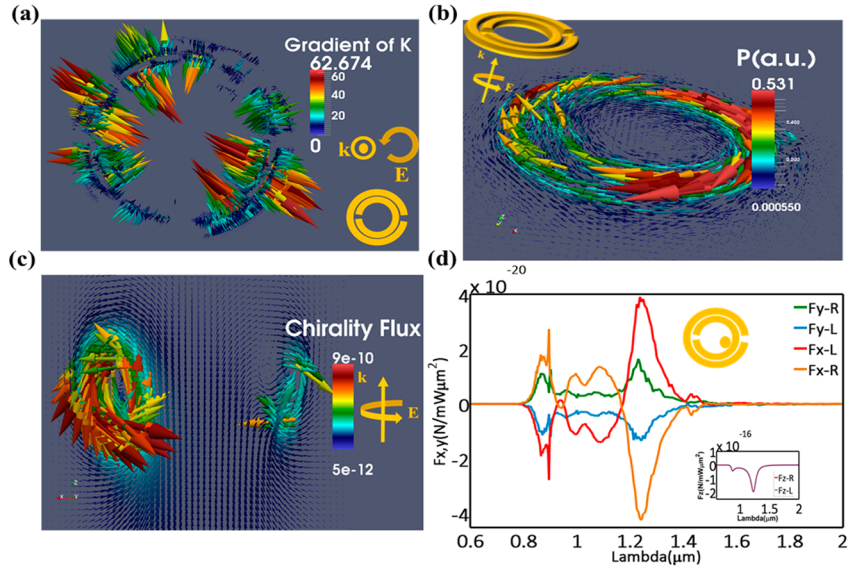

Figure 5. (a) Gradient of optical chirality, *K*, at λ = 1258 nm in the *xy*-plane. The gradient vector field is mostly confined to the plane perpendicular to the energy flow and linear momentum of the EM field. (b) Bird's eye view of the Poynting vector at λ = 1404 nm shows that the optical energy circulates preferentially in-plane with the DSRR. (c) Vector field of the chirality flux at λ = 1404 nm in the *xz*-plane, perpendicular to the DSRR. This flux is asymmetric and highly localized. (d) Calculated force components for a chiral dipole. The position of the dipole is shown in the inset and was chosen to maximize the chiral contribution to the force. Right-handed and left-handed chiral dipoles are denoted with R and L, respectively.

sign. This can be clearly seen in Figure 4e, where chirality enhancement is plotted for two different spots inside the DSRR. The negative peak of the chiral enhancement is red-shifted relative to the dipolar electric resonance, whereas the positive peak is blue-shifted. For the wavelengths between the electric dipole resonance at λ = 1420 nm and the magnetic quadruple resonance at λ = 1070 nm a broadband positive chiral enhancement is observed. Beyond the dominant magnetic resonance at 1070 nm additional weaker magnetic modes are excited, which give rise to weaker enhancements. Finally, it should be mentioned that this spectral tunability of chiral enhancement, which solely depends on the excitation

DOI: 10.1021/ph500399k
ACS Photonics 2015, 2, 361−368

wavelength and not the type of circular polarization of the incident wave, adds to the potential of DSRRs for chiral sensing schemes.

Chirality Density Gradient and Chirality Flux near the DSRR. So far we have focused on optical chirality near the DSRR and on the design considerations to generate same-sign chiral fields. Recently there has been an increasing interest in a novel chiral biosensing scheme which is based on enantiomer-selective separation of a racemic mixture through chiral forces.[33−39] The fundamental mechanism underlying an enantiomer-selective separation is the creation of experimental conditions under which chiral objects with different handedness experience forces in opposite directions. In the linear and harmonic regime a chiral dipole can be described by[33] $\boldsymbol{P} = \alpha\boldsymbol{E} + i\chi\boldsymbol{H}$,$\boldsymbol{m} = -i\chi\boldsymbol{E} + \beta\boldsymbol{H}$, where α is the complex electric polarizability, β is the complex magnetic polarizability, and χ is the electro-magnetic dipole polarizability, which we call the chirality factor. Due to such electric-magnetic mixing through χ, a chiral dipole in a gradient field will experience not only the usual achiral gradient force, but also a chiral force. Such a chiral force can be decomposed into a reactive and dissipative parts which depend on the real and imaginary parts of the complex χ respectively. The reactive chiral force can be written as[33] $\langle \mathbf{F}^{r}_{\chi} \rangle = \mathrm{Re}[c\chi](c/\omega)(\nabla K)$, where c is the speed of light. Since two enantiomers have χ-values of opposite signs, they will experience forces of the opposite sign. As is evident from the expression for reactive chiral force, a large optical chirality gradient is required to realize such a chiral force. Our main purpose in this section is to propose a new approach for chiral trapping based on plasmonic effects and not interference-based mechanisms.[33] In such schemes a precise interference of counter-propagating beams is utilized to create local chiral gradient fields, which are in general weak. To demonstrate that in principle the idea of plasmonically generated chiral forces can be an alternative to the previously proposed schemes, we first calculated the gradient of optical chirality density around the DSRR at λ = 1258 nm (Figure 5a). The preferential radial orientation of the chiral density gradient is in sharp contrast to that of Poynting vector (Figure 5b) and linear momentum of light. The individual chiral gradient vectors point mostly inward (outward) for the inner ring (outer ring). It can be seen in Figure 5a that, in an ideal experimental case, the enantiomers on the boundary will experience opposite chiral gradient forces and as long as the competing achiral forces are smaller, at least in some directions, one can realize enantio-separation.

In the next step, we calculated the forces exerted on chiral dipoles of opposite handedness using Maxwell's Stress Tensor. We simulated the chiral dipoles with a combination of parallel (antiparallel) electric and magnetic dipoles which represents a left-handed (right-handed) helical molecule.[40] The excitation frequency of the dipole was centered at 1070 nm to couple most efficiently to the dominant quadruple magnetic resonance of the DSRR. The chiral dipoles were placed inside the DSRR at the marked position in the inset of Figure 5d and were located 5 nm above the DSRR. The DSRR was excited by circularly polarized light. In order to minimize the competing achiral gradient force components in the DSRR plane, we chose the electric and magnetic dipoles in z direction. For the chosen chiral dipole, $p \propto m$ and $\mathrm{Im}[\chi] \ll \mathrm{Re}[\chi]$.[33,41−43] Figure 5d shows the calculated force components as a function of the excitation wavelength. As we expected, the dipoles couple most efficiently to the magnetic modes of the DSRR. This is of crucial significance in minimizing plasmonic achiral gradient forces, which peak at the electric resonances. F_x and F_y, which lie in the DSRR plane, show opposite signs for two enantiomers. Interestingly, they peak at the wavelengths for which highest chiral enhancements occur. This is a consequence of the fact that the chiral force depends on the gradient of the chirality density and not the electric (magnetic) energy density. This exciting result, however, should be considered together with the dominant achiral force in the z direction, which is 3−4 orders of magnitude larger than the in-plane chiral forces and is of the same magnitude for both enantiomers. This is plotted in the inset of Figure 5d. Unlike the chiral forces, F_z peaks at the electric dipole resonance of the structure where a giant downward gradient force is exerted to both enantiomers of a chiral dipole and dominates over any chiral force in this direction. This means that in a hypothetical experiment both enantiomers would get trapped in the DSRR plane due to this large downward gradient force. At the same time, both enantiomers experience opposite chiral forces in x and y directions and would, therefore, physically separate. This example demonstrates the potential of plasmonically generated chiral forces in enantio-separation schemes. It should be noted, however, that the DSRRs may not be the ideal plasmonic structure to generate largest chiral gradient forces while minimizing the achiral gradient forces. The optimization of this effect needs to be investigated further and is beyond the scope of this manuscript.

The reactive chiral force discussed above is determined by the chiral density gradient, whereas the dissipative chiral force is given as $\langle \mathbf{F}^{d}_{\chi} \rangle = \mathrm{Im}[c\chi](2/c)(\boldsymbol{\Phi} - \nabla \times \boldsymbol{\Pi}/2)$,[33] where $\boldsymbol{\Phi} = \{\tilde{\mathbf{E}} \times (\nabla \times \tilde{\mathbf{B}}) - \tilde{\mathbf{B}} \times (\nabla \times \tilde{\mathbf{E}})\}/2$ is the chirality flow, where $\tilde{\mathbf{E}}$ and $\tilde{\mathbf{B}}$ are the real parts of the electric and magnetic fields and $\boldsymbol{\Pi} = 1/2\ \mu_0 \mathrm{Re}[\boldsymbol{E} \times \boldsymbol{B}^*]$ is the time-averaged Poynting vector. The dissipative nature of this force arises from the out-of-phase component of χ.[33] The direct relationship between the dissipative force and chirality flow suggests that a large chirality flow will boost the interaction between light and chiral biomolecules. To show the behavior of chirality flow near the DSRR we simulated Φ for λ = 1404 nm. In the immediate surroundings and inside the DSRR, there is a dramatic discrepancy in the behavior of chirality flow and EM energy flow. The Poynting vector is azimuthal and lies in the DSRR plane (Figure 5b). The orientation of the Poynting vector is largely determined by the strong capacitive coupling of the inner and outer rings, which results in a preferential radial orientation of the $\boldsymbol{E}$-field in the gap between them. In contrast, the $\boldsymbol{H}$-field stemming from the LC resonances points mostly out of plane. Unlike the energy flow described by the Poynting vector, the chirality flow curls on a spiral-like trajectory around the DSRR rings (Figure 5c). Such spatial orientation of chirality flow is closely connected to the definition of chirality momentum density.[44] Also, the asymmetry of the charge distribution in the DSRR leads to an asymmetric localization of the chirality flow. A chirality flow centered in a confined spatial domain can be highly advantageous in limiting the chiral interactions between the incident light and chiral molecules to a predetermined location in space that contains such confined enhanced chirality flow. Metamaterials with these properties would be of significant interest in chiral biosensing and imaging.

To conclude, we proposed making use of bianisotropic metamaterials to generate chiral fields and forces. In particular, we investigated the behavior of optical chirality density and optical chirality flow around DSRRs. We demonstrated the

DOI: 10.1021/ph500399k
ACS Photonics 2015, 2, 361−368

potential of DSRRs to generate same-sign chiral near field in their surroundings. The enhanced chiral near-field remains of uniform-sign over a large region in the center of the DSRRs, where it is easily accessible by chiral biomolecules. Furthermore, it was demonstrated that DSRRs are versatile substrates for enantioselective separation schemes based on the idea of chiral forces. We have shown that these well-known metamaterials can create high gradients of optical chirality as well as highly localized and enhanced chirality flows.

AUTHOR INFORMATION

Corresponding Authors

*E-mail: halizade@bu.edu (M.H.A.).
*E-mail: bmr@bu.edu (B.J.R.).

Notes

The authors declare no competing financial interest.

ACKNOWLEDGMENTS

This work was supported by the U.S. Department of Energy, Office of Basic Energy Sciences, Division of Materials Science and Engineering under Award DOE DE-SC0010679. The authors acknowledge fruitful discussions with Yan Hong.

REFERENCES

(1) Smithells, R.; Newman, C. Recognition of thalidomide defects. *J. Med. Genet.* **1992**, *29*, 716.
(2) Fischer, E. Ueber die configuration des traubenzuckers und seiner isomeren. *Ber. Dtsch. Chem. Ges.* **1891**, *24*, 1836.
(3) Lipkin, D. Existence of a new conservation law in electromagnetic theory. *J. Math. Phys.* **1964**, *5*, 696.
(4) Fasman, G. D. *Circular Dichroism and the Conformational Analysis of Biomolecules*; Plenum Press: New York, 1996.
(5) Tang, Y.; Cohen, A. E. Optical chirality and its interaction with matter. *Phys. Rev. Lett.* **2010**, *104*, 163901.
(6) Tang, Y.; Cohen, A. E. Enhanced enantioselectivity in excitation of chiral molecules by superchiral light. *Science* **2011**, *332*, 333.
(7) Hendry, E.; Carpy, T.; Johnston, J.; Popland, M.; Mikhaylovskiy, R. V.; Lapthorn, A. J.; Kelly, S. M.; Barron, L. D.; GadegaardN; KadodwalaM. Ultrasensitive detection and characterization of biomolecules using superchiral fields. *Nat. Nanotechnol.* **2010**, *5*, 783.
(8) Govorov, A. O.; Fan, Z.; Hernandez, P.; Slocik, J. M.; Naik, R. R. Theory of circular dichroism of nanomaterials comprising chiral molecules and nanocrystals: plasmon enhancement, dipole interactions, and dielectric effects. *Nano Lett.* **2010**, *10*, 1374.
(9) Fan, Z.; Govorov, A. O. Plasmonic circular dichroism of chiral metal nanoparticle assemblies. *Nano Lett.* **2010**, *10*, 2580.
(10) Kuzyk, A.; Schreiber, R.; Fan, Z.; Pardatscher, G.; Roller, E.-M.; Hogele, A.; Simmel, F. C.; Govorov, A. O.; Liedl, T. DNA-based self-assembly of chiral plasmonic nanostructures with tailored optical response. *Nature* **2012**, *483*, 311.
(11) García-Etxarri, A.; Dionne, J. A. Surface-enhanced circular dichroism spectroscopy mediated by nonchiral nanoantennas. *Phys. Rev. B* **2013**, *87*, 235409.
(12) Meinzer, N.; Hendry, E.; Barnes, W. L. Probing the chiral nature of electromagnetic fields surrounding plasmonic nanostructures. *Phys. Rev. B* **2013**, *88*, 041407.
(13) Schäferling, M.; Yin, X.; Giessen, H. Formation of chiral fields in a symmetric environment. *Opt. Express* **2012**, *20*, 26326−26336.
(14) Davis, T. J.; Hendry, E. Superchiral electromagnetic fields created by surface plasmons in nonchiral metallic nanostructures. *Phys. Rev. B* **2013**, *87*, 085405.
(15) Schäferling, M.; Dregely, D.; Hentschel, M.; Giessen, H. Tailoring enhanced optical chirality: design principles for chiral plasmonic nanostructures. *Phys. Rev. X* **2012**, *2*, 031010.
(16) Schäferling, M.; Yin, X.; Engheta, N.; Giessen, H. Helical plasmonic nanostructures as prototypical chiral near-field sources. *ACS Photonics* **2014**, *1*, 530.
(17) Yoo, S.; Cho, M.; Park, Q. H. Globally enhanced chiral field generation by negative-index metamaterials. *Phys. Rev. B* **2014**, *89*, 161405.
(18) Shelby, R. A.; Smith, D. R.; Schultz, S. Experimental verification of a negative index of refraction. *Science* **2001**, *292*, 77.
(19) Baena, J. D.; Bonache, J.; Martin, F.; Sillero, R. M.; Falcone, F.; Lopetegi, T.; Laso, M. A. G.; Garcia-Garcia, J.; Gil, I.; Portillo, M. F.; Sorolla, M. Equivalent-circuit models for split-ring resonators and complementary split-ring resonators coupled to planar transmission lines. *IEEE Trans. Microwave Theory Tech.* **2005**, *53*, 1451.
(20) Marques, R.; Mesa, F.; Martel, J.; Medina, F. Comparative analysis of edge- and broadside-coupled split ring resonators for metamaterial design: theory and experiments. *IEEE Trans. Antennas Propag.* **2003**, *51*, 2572.
(21) Marqués, R.; Medina, F.; Rafii-El-Idrissi, R. Role of bianisotropy in negative permeability and left-handed metamaterials. *Phys. Rev. B* **2002**, *65*, 144440.
(22) Kriegler, C. E.; Rill, M. S.; Linden, S.; Wegener, M. Bianisotropic photonic metamaterials. *IEEE J. Sel. Top. Quantum Electron.* **2010**, *16*, 367.
(23) Smith, D. R.; Gollub, J.; Mock, J. J.; Padilla, W. J.; Schurig, D. Calculation and measurement of bianisotropy in a split ring resonator metamaterial. *J. Appl. Phys.* **2006**, *100*, 024507.
(24) Katsarakis, N.; Koschny, T.; Kafesaki, M.; Economou, E. N.; Soukoulis, C. M. Electric coupling to the magnetic resonance of split ring resonators. *Appl. Phys. Lett.* **2004**, *84*, 2943.
(25) Corrigan, T. D.; Kolb, P. W.; Sushkov, A. B.; Drew, H. D.; Schmadel, D. C.; Phaneuf, R. J. Optical plasmonic resonances in split-ring resonator structures: an improved LC model. *Opt. Express* **2008**, *16*, 19850.
(26) Rockstuhl, C.; Lederer, F.; Etrich, C.; Zentgraf, T.; Kuhl, J.; Giessen, H. On the reinterpretation of resonances in split-ring-resonators at normal incidence. *Opt. Express* **2006**, *14*, 8827.
(27) Zhou, J.; Koschny, T.; Soukoulis, C. M. Magnetic and electric excitations in split ring resonators. *Opt. Express* **2007**, *15*, 17881.
(28) Chen, C.-Y.; Wu, S.-C.; Yen, T.-J. Experimental verification of standing-wave plasmonic resonances in split-ring resonators. *Appl. Phys. Lett.* **2008**, *93* (3), 034110.
(29) Hou, Y. Which is the interpretation of plasmon resonance in 2D split-ring resonator structure—standing wave or LC circuit? *Plasmonics* **2013**, *8*, 665.
(30) Gay-Balmaz, P.; Martin, O. J. F. Electromagnetic resonances in individual and coupled split-ring resonators. *J. Appl. Phys.* **2002**, *92*, 2929.
(31) Johnson, P. B.; Christy, R. W. Optical constants of the noble metals. *Phys. Rev. B* **1972**, *6*, 4370.
(32) Klein, M. W.; Enkrich, C.; Wegener, M.; Soukoulis, C. M.; Linden, S. Single-slit split-ring resonators at optical frequencies: limits of size scaling. *Opt. Lett.* **2006**, *31*, 1259.
(33) Antoine, C.-D.; James, A. H.; Cyriaque, G.; Thomas, W. E. Mechanical separation of chiral dipoles by chiral light. *New J. Phys.* **2013**, *15*, 123037.
(34) Tkachenko, G.; Brasselet, E. Optofluidic sorting of material chirality by chiral light. *Nat. Commun.* **2014**, *5*, 3577.
(35) Robert, P. C.; Stephen, M. B.; Alison, M. Y. Discriminatory optical force for chiral molecules. *New J. Phys.* **2014**, *16*, 013020.
(36) Cameron, R. P.; Yao, A. M.; Barnett, S. M. Diffraction gratings for chiral molecules and their applications. *J. Phys. Chem. A* **2014**, *118*, 3472.
(37) Tkachenko, G.; Brasselet, E. Helicity-dependent three-dimensional optical trapping of chiral microparticles. *Nat. Commun.* **2014**, *5*, 4491.
(38) Wang, S. B.; Chan, C. T. Lateral optical force on chiral particles near a surface. *Nat. Commun.* **2014**, *5*, 3307.
(39) Ding, K.; Ng, J.; Zhou, L.; Chan, C. T. Realization of optical pulling forces using chirality. *Phys. Rev. A* **2014**, *89*, 063825.

DOI: 10.1021/ph500399k
ACS Photonics 2015, 2, 361−368

(40) Klimov, V. V.; Guzatov, D. V.; Ducloy, M. Engineering of radiation of optically active molecules with chiral nano-meta-particles. *Europhys. Lett.* **2012**, *97*, 47004.
(41) Eisele, D. M.; Knoester, J.; Kirstein, S.; Rabe, J. P.; Vanden Bout, D. A. Uniform exciton fluorescence from individual molecular nanotubes immobilized on solid substrates. *Nat. Nanotechnol.* **2009**, *4*, 658−663.
(42) Liu, N.; Liu, H.; Zhu, S.; Giessen, H. Stereometamaterials. *Nat. Photonics* **2009**, *3*, 157−162.
(43) Yan, W.; Xu, L.; Xu, C.; Ma, W.; Kuang, H.; Wang, L.; Kotov, N. A. Self-assembly of chiral nanoparticle pyramids with strong R/S optical activity. *J. Am. Chem. Soc.* **2012**, *134*, 15114.
(44) Bliokh, K. Y.; Nori, F. Characterizing optical chirality. *Phys. Rev. A* **2011**, *83*, 021803.

DOI: 10.1021/ph500399k
ACS Photonics 2015, 2, 361−368